Bioelectromagnetics 35:580–597 (2014)

Dosimetric Study of Fetal Exposure to Uniform Magnetic Fields at 50 Hz

Ilaria Liorni,[1,2]* Marta Parazzini,[1] Serena Fiocchi,[1] Mark Douglas,[3] Myles Capstick,[3] Marie-Christine Gosselin,[3,4] Niels Kuster,[3,4] and Paolo Ravazzani[1]

[1]CNR Consiglio Nazionale delle Ricerche, Istituto di Elettronica e di Ingegneria dell'Informazione e delle Telecomunicazioni IEIIT (CNR National Research Council of Italy, Institute of Electronics, Computer and Telecommunication Engineering), Piazza Leonardo da Vinci, Milano, Italy

[2]Dipartimento di Elettronica, Informazione e Bioingegneria DEIB (Department of Electronics, Information and Bioengineering), Politecnico di Milano, Piazza Leonardo da Vinci, Milano, Italy

[3]Foundation for Research on Information Technologies in Society (IT'IS Foundation), Zurich, Switzerland

[4]Swiss Federal Institute of Technology (ETHZ), Zurich, Switzerland

In this paper, fetal exposure to uniform magnetic fields (MF) with different polarizations is quantified at 50 Hz. Numerical computations were performed on high-resolution pregnant models at 3, 7, and 9 months of gestational age (GA), that distinguish a high number of fetal tissues. Fetal whole-body and tissue-specific induced electric fields (*E*) and current densities (*J*) were analyzed as a function of both the extremely low frequency magnetic field (ELF-MF) polarization and GA. Additionally, the induced field variation due to changes in fetal position was analyzed by means of two new pregnant models. The uncertainty budget due to the grid resolution was also calculated. Finally, the compliance of the fetal exposure to the ICNIRP Guidelines was checked. A fetal exposure matrix was built at 50 Hz, which could be used to further investigate possible interaction mechanisms between ELF-MF and the associated health risk. Some specific findings were: (1) the induced fields increased with GA; (2) the maxima E were found in skin and fat tissues at each GA; (3) fetal tissue-specific exposure was modified as a function of GA and polarization; (4) the change of the fetal position in the womb significantly modified the induced E in some fetal tissues; (5) the induced fields were in compliance with ICNIRP Guidelines and the results were quite below the permitted threshold limit. Bioelectromagnetics 35:580–597, 2014.
© 2014 Wiley Periodicals, Inc.

Key words: pregnant woman exposure; ELF magnetic fields; numerical dosimetry

INTRODUCTION

There is increasing concern regarding the safety of extremely low-frequency magnetic fields (ELF-MF) and their possible effects on the health of children from prenatal life to adolescence. Much of the scientific research examining long-term risks from ELF-MF exposure has focused on childhood leukemia [WHO, 2007a]. Several meta-analyses consistently found statistically significant increased relative risk estimates for childhood leukemia for ELF-MF exposure above 0.4 μT [Ahlbom et al., 2000; Greenland et al., 2000; Kheifets et al., 2010]. However, the epidemiological evidence is weakened by methodological problems, such as potential selection bias [Schüz and Ahlbom, 2008]. In addition, there are no accepted biophysical mechanisms that would suggest that low-level exposures are involved in cancer development [Ahlbom et al., 2008]. Thus, if there were any effects from exposures to these low-level fields, it would have to be through a biological mechanism that is as yet unknown [WHO, 2007a]. In order to provide a better

Grant sponsor: European Union's Seventh Programme for Research, Technological Development and Demonstration; grant number: 282891.

*Correspondence to: Ilaria Liorni, CNR Consiglio Nazionale delle Ricerche, Istituto di Elettronica e di Ingegneria dell'Informazione e delle Telecomunicazioni IEIIT, Piazza Leonardo da Vinci, Milano, Italy. E-mail: ilaria.liorni@ieiit.cnr.it

Received for review 1 February 2014; Accepted 24 July 2014

DOI: 10.1002/bem.21878
Published online 29 September 2014 in Wiley Online Library (wileyonlinelibrary.com).

© 2014 Wiley Periodicals, Inc.

understanding of this topic WHO [2007b] indicated as an urgent priority in the Research Agenda for ELF-MF, the estimation of the induced electric fields and current densities within human tissues due to ELF-MF exposure to help reveal plausible biological mechanisms of interaction and, particularly, to assess possible enhancements of these induced fields during fetal development in relation to childhood leukemia.

Until now, dosimetric studies have been performed mainly with human models of adults [Gandhi et al., 2001; Hirata et al., 2001; Dimbylow, 2005; Leitgeb et al., 2008]. A few studies considered the ELF-MF exposure of children [Dimbylow and Findlay, 2010; Bakker et al., 2012] and some work has been carried out on pregnant woman and fetuses with appropriate anatomical modeling [Dimbylow, 2006; Cech et al., 2007; Zupanic et al., 2007; Dimbylow and Findlay, 2010; Zoppetti et al., 2011]. The first numerical models of pregnant women were based on a fetus [Kainz et al., 2003; Hand et al., 2006], modeled with a 20 cm diameter sphere. In Kainz et al. [2003], the fetal model was inserted in a simplified 34-week-pregnant woman model, whereas in Hand et al. [2006], it was represented in an anatomically realistic abdominal model taken from magnetic resonance imaging (MRI) data of a 28-week-pregnant woman. After that, some hybrid voxel-mathematical models of pregnant women at different stages of pregnancy were developed in Dimbylow [2006]. More specifically, in that study, models of the embryo and fetus at 8, 13, 26, and 38 weeks of gestation were combined with an anatomically realistic adult female model [Dimbylow, 2005]. These pregnant woman models were segmented into more than 45 different tissues and organs, in which, the whole fetus and the fetal organs (only the brain and skeleton were available) were modeled by spherical or cylindrical shapes. In particular, the brain was represented as a sphere in the embryonic period (8 weeks), whereas the skeleton was introduced only in the late stages of pregnancy. In Cech et al. [2007], a pregnant woman model was derived from a combination of a trunk model generated from X-ray computed tomography images of a 30-week-pregnant woman [Shi and Xu, 2004], of the central nervous system (brain and spinal cord) of a male model [Dimbylow, 2002] and a homogeneous whole-body three-dimensional (3-D) computer-generated model of a woman. In this model, only fetal skeleton and fetal soft tissues could be distinguished. After that, in Nagaoka et al. [2007], an anatomically realistic whole-body-pregnant woman was obtained by combining a new fetus voxel model (developed on the basis of abdominal MRI data from a 26-week-pregnant woman) and a deformed model developed from a non-pregnant adult Japanese woman model. In this pregnant woman model, the fetus was characterized as fetal whole-body, fetal brain, fetal eye, amniotic fluid, placenta and uterine wall. In Xu et al. [2007] the Renssealer Polytechnic Institute pregnant females models (RPI-P) were developed using a boundary representation modeling approach. The set of models represented the pregnant women at 13, 26, and 38 weeks of pregnancy. Three anatomical tissues of the fetus were considered: the brain, skeleton and soft tissue. In Bibin et al. [2010], hybrid whole-body pregnant woman models were developed, with detailed fetal anatomy extracted from 3-D ultrasonic and MRI image data. In particular, depending on the age of the fetus, the fetus envelope, and some fetal tissues (i.e., eyes, brain, urinary bladder, lungs, heart, uterus, amniotic fluid, and umbilical cord) were extracted from the MRI images. However, in this study, maternal body was represented as a single homogeneous tissue.

In Christ et al. [2012], high-resolution pregnant woman models at 3, 7, and 9 months of pregnancy were developed, based on the computer-aided design representation of the organ surfaces. In that study, the exposure to induction cookers for sources close to the pregnant woman body at 20 kHz was addressed by means of a tissue-to-tissue approach. The pregnant woman models were based on the model "Ella" of the Virtual Family [Christ et al., 2010], in which endogenous fetus models were included. The model "Ella" represents a 26-years-old woman, in which more than 80 tissue-types have been segmented. At 3 months of gestational age (GA), 15 tissues were distinguished in the fetal model developed on the base of images available in the literature. The fetal model was integrated into the womb of "Ella," which was scaled to accommodate the fetus. At 7 months, the fetus has 17 tissues and the model was developed from MR-images of the torso of pregnant woman, while at 9 months GA, the pregnant woman model was based on a 7-month-old, but the fetus model was replaced with a scaled newborn. In this latter case, 26 fetal tissues were distinguished.

This study, using an approach in terms of human models similar to Christ et al. [2012], aimed to assess the fetal whole-body and tissue-specific induced fields at different gestational ages (GA), exposed to uniform magnetic fields at 50 Hz. The whole-body and tissue-specific induced fields were analyzed at each of the three considered stages of pregnancy as a function of GA and of three different magnetic field polarizations. The amplitude of the magnetic field was chosen after analyzing the existing literature about the ELF-MF personal and residential exposure measurements [Schüz et al., 2000; Brix et al., 2001; Grellier et al.,

2014]. In all these studies, the median over 24 h was always found lower than 1 μT, so this MF amplitude can be considered a reasonable maximum value to use for the evaluation of the personal exposure.

Moreover, considering different legislations in various countries, when regulating the exposure levels at 50 Hz, one can find maximum exposure levels of a few μT. In Switzerland, for example, the median over 24 h should be less than 1 μT in places in which the person remains for more than 4 h. In Italy, the median over 24 h of the level of magnetic field at 50 Hz would be less than to 3 μT for the new power lines in places, in which the person remains for more than 4 h.

A detailed analysis is also provided for the fetal bone tissue exposure to ELF-MF. This problem was already investigated from a subcellular perspective in Chiu and Stuchly [2005], where two models of bone marrow substructures exposed to electric fields at the power-line frequencies were computed numerically. The interest in the analysis of the fetal bone exposure is due to the fact that the bone marrow is one of the possible tissues in which the first insult of the childhood leukemia might start [Pui et al., 2008].

Furthermore, the dependence of fetal exposure on the fetal position in the womb has been investigated by means of two additional pregnant woman models, in which the fetus at 3 months GA has been rotated in the womb with respect to the original model used in this study. The uncertainty on the fetal grid discretization has also been calculated using the pregnant model at 7 months GA. Finally, in order to generalize the conclusions of this work, the incident fields at the fetus have been scaled to the levels of the ICNIRP Guidelines [1998, 2010] at 50 Hz and an analysis of the compliance to the basic restrictions has been carried out.

MATERIALS AND METHODS

Numerical Exposure Modeling

Simulations were conducted using the Magneto Quasi-Static low frequency solver of the simulation platform SEMCAD X v. 14.8.4 (Schmid & Partner Engineering, Zürich, Switzerland), which uses a Biot–Savart solver and is based on the scalar potential finite element (SPFE) method. In the low frequency range, where the pertinent dimensions of the computational domain are smaller than the free space wavelength, the magnetic vector potential $\boldsymbol{A}$ is decoupled from the electric field $\boldsymbol{E}$ and can be calculated using Biot-Savart's law. Furthermore, since in the human body the displacement current is neglected with respect to the conduction current for the exposure condition here studied ($\sigma \gg j\omega\varepsilon$ where σ and ε are the electrical conductivity and the permittivity of the tissues, respectively, and ω is the angular frequency of the field), $\boldsymbol{E}$ can be calculated from the scalar potential ϕ by:

$$-\nabla \cdot \sigma \nabla \Phi = j\omega \nabla \cdot (\sigma \boldsymbol{A}). \quad (1)$$

whereas, the finite element method is used to solve for Φ. Rectilinear grids were applied to discretize the complex anatomical models.

Numerical Models of Pregnant Women

Three pregnant woman anatomical whole-body models at 3, 7, and 9 months GA based on the model "Ella" of the Virtual Family [Christ et al., 2010] and made available for research purposes through the IT'IS Foundation were used for the dosimetric analysis. These models consist of a model of non-pregnant "Ella" [Christ et al., 2010], which was augmented to account for changes in the female body due to pregnancy (the presence of the fetus and enlargement of the breast). A detailed description of the construction of the models is given in Christ et al. [2012]. The mass of the fetus models at the three gestational ages are 15, 1700, and 2700 g. In the models, up to 80 different tissue types are represented (up to 26 in the fetus models). Due to the formation of the organs at different stages of pregnancy, not all three models of the fetus distinguish the same tissues. In particular 15, 17, and 26 different tissues can be distinguished at 3, 7, and 9 months GA, respectively. Details on the fetal tissues at each gestational age can be found in Table 2. Figure 1 shows the three pregnant woman models used in the study.

Two additional pregnant woman models at 3 months GA, based on "Ella" model, were made available by IT'IS Foundation, in which the fetus and placenta were rotated with respect to the original position in the woman's womb and adjusted to fit into the uterus. The two additional positions were selected on the basis of the most statistically significant positions that a fetus can take at that stage of pregnancy. In Figure 2, three positions of the fetus in a womb are represented. Posture A refers to the 3-month-old GA fetus also represented in Figure 1, and used to perform the analysis of the induced fields across this study.

Grid Resolution

Pregnant woman tissues (both woman and fetus) at 7 and 9 months GA were discretized with a grid resolution of 1 mm. At 3 months GA, the fetal tissues

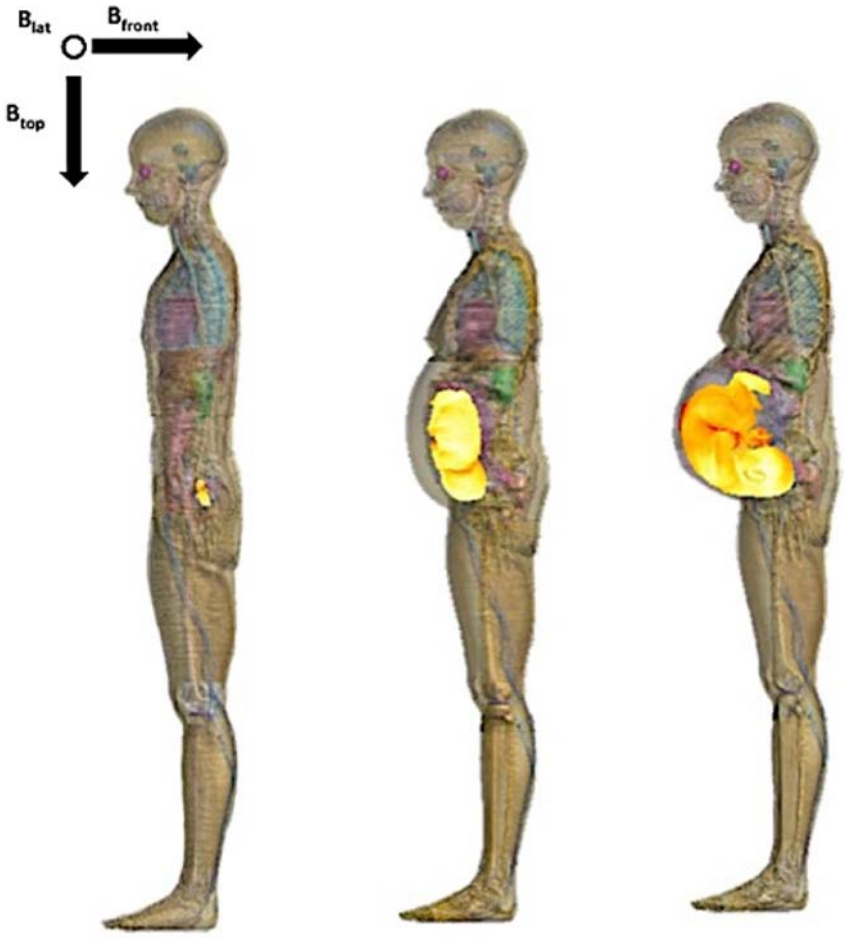

Fig. 1. From left to right, pregnant woman models at 3, 7, and 9 months GA, respectively. At each stage of pregnancy, the fetus in the woman's womb has been highlighted. The polarization of the incident ***B***-field (B_{front}, B_{lat}, B_{top}) is represented with respect to the pregnant woman's body.

were discretized with a grid resolution of 0.3 mm because of the thickness of the fetal skin.

Conductivities of Tissues

The woman and fetal tissue conductivities (Tables 1 and 2, respectively) chosen in this study were already used in Liorni et al. [2013]. The conductivities of most of the woman tissues were assigned according to data available in the literature [Gabriel et al., 1996a,b,c, 2009; Hasgall et al., 2012]. The skin conductivity was set to 0.1 S/m to take into account the higher conductivity of deeper granular tissue, that is, dermis [Dimbylow, 2005]. Furthermore, an average value between gray matter and white matter conductivities was assigned to medulla oblongata, pons and midbrain tissues. The conductivity of the amniotic fluid was set equal to 1.28, 1.27, and 1.10 S/m at 3, 7, and 9 months GA, respectively, whereas the conductivity of the placenta was the same as that of the blood (0.7 S/m) [De Luca et al., 1996; Dimbylow, 2006; Peyman et al., 2011].

The fetal conductivity values were set equal to those of an adult except for brain, bone, and fat tissues. The lowest conductivity (0.185 S/m) for woman brain tissues was assigned to the fetal brain from a conservative point of view, to obtain higher conductivity contrast with the embedding cerebrospinal fluid (CSF). The bone tissue conductivity was taken as a weighted average of bone and blood (to take into consideration the infiltration of bone marrow at a very young age), and fat conductivity was set at 0.12 S/m, estimated as a blend between fat and muscle conductivities, according to the suggestion of Peyman et al. [2009], because of the higher water content and blood presence at very young age. Other studies [Dimbylow, 2006; Cech et al., 2007; Zupanic et al., 2007] also considered the changing of the fetal tissue

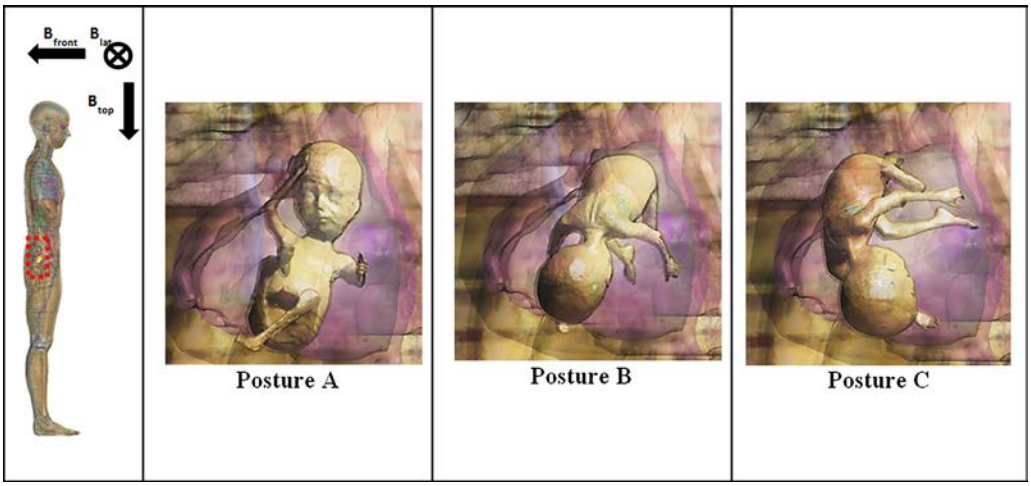

Fig. 2. Different positions assumed by the 3 months GA fetus in pregnant woman's womb. Each figure has been taken from pregnant woman's lateral side. Fetus in Posture A is the same as that one used in the induced field analysis. Posture A was used as a reference to quantify the changes with respect to the other postures. Fetuses in Posture B and C belong to the two additional pregnant woman models used in this study to assess the influence of the variation of the fetal posture. On the left side of the figure, the polarization of the incident $\boldsymbol{B}$-field (B_{front}, B_{lat}, and B_{top}) respect to the woman's body is represented and the fetus in woman's womb has been highlighted.

conductivities with respect to the adults following different approaches than the one proposed in this study.

Exposure Configurations

Three orthogonal polarizations of 1 μT magnetic field at the frequency of 50 Hz were studied, resulting on "Ella's" body in a front-to-back, lateral (left-to-right) and top-to-bottom exposure (B_{front}, B_{lat}, B_{top}, respectively). The vector potential $\boldsymbol{A}$ and the magnetic flux density $\boldsymbol{B}$ were set to obtain a magnetic field perfectly homogeneous for all the polarizations.

Uncertainty Evaluation

The uncertainty budget of the fetal exposure due to fetal grid resolution was carried out following the guidelines in Taylor and Kuyatt [1994] and the International Organization for Standardization/International Electrotechnical Commission (ISO/IEC) [2008]. The uncertainty evaluation was performed on the $E_{\text{av,99th}}$, $E_{\text{av,peak}}$, and the $J_{\text{av,peak}}$, for a Gaussian normal distribution. The uncertainty was expanded with a coverage factor $k = 2$, which corresponds to a level of confidence equal to 95%. The analysis was performed only on the 7 months GA fetus, in which fetal tissues grid resolution was varied from 0.6 to 1.2 mm with a step of 0.1 mm, considering all three orthogonal polarizations (B_{front}, B_{lat}, and B_{top}) previously described.

Exposure Assessment of Pregnant Women and Fetuses

The fetal exposure was assessed in terms of induced electric field and current density both in the whole-body fetus and in each tissue. The electric field averaged ($\boldsymbol{E_{av}}$) on a cube of $2 \times 2 \times 2\,\text{mm}^3$ [ICNIRP, 2010] was analyzed. If $2 \times 2 \times 2\,\text{mm}^3$ of continuous tissue cannot be found (e.g., in the skin and in the retina), the averaging is performed over a smaller volume that contains only the specific tissue being analyzed. Furthermore, the current density averaged on a cross-section of $1\,\text{cm}^2$ ($\boldsymbol{J_{av}}$) perpendicular to the direction of the current [ICNIRP, 1998] was extracted. Also, if the cross-section of a tissue is lower than $1\,\text{cm}^2$, the averaging is done on a cross-section as large as possible. For both quantities, the root mean square of $\boldsymbol{E_{av}}$ and $\boldsymbol{J_{av}}$ was calculated. The 50th and 99th percentiles and the peak value of E_{av} were extracted ($E_{\text{av,50th}}$, $E_{\text{av,99th}}$, $E_{\text{av,peak}}$, respectively), as well as the 50th percentile and peak value of J_{av} ($J_{\text{av,50th}}$, $J_{\text{av,peak}}$). The induced electric field and current density was also evaluated in terms of their mean across the three polarizations, and denoted with the acronym "map."

Compliance to the ICNIRP Guidelines

The results previously obtained have been scaled to check compliance with the limits suggested by the ICNIRP Guidelines [1998, 2010] for the general public. In particular, in the ICNIRP Guidelines [1998]

TABLE 1. Woman Tissue Conductivities

Woman tissue	σ [S/m]	Refs.	Woman tissue	σ [S/m]	Refs.
Adrenal gland	0.521	Gabriel et al. [1996a,b,c] (source: gland)	Uterus	0.229	Gabriel et al. [1996a,b,c]
Artery	0.650	Hasgall et al. [2012]	Vagina	0.0545	Gabriel et al. [1996a,b,c]
Bone	0.095	Hasgall et al. [2012]	Vein	0.650	Hasgall et al. [2012] (source: blood)
Cartilage	0.171	Gabriel et al. [1996a,b,c]	Vertebrae	0.095	Hasgall et al. [2012] (source: bone)
Connective tissue	0.270	Gabriel et al. [1996a,b,c]	Air internal	0	Gabriel et al. [1996a,b,c]
Bladder	0.205	Gabriel et al. [1996a,b,c]	Brain gray matter	0.185	Hasgall et al. [2012]
Fat	0.078	Gabriel et al. [2009]	Brain white matter	0.369	Hasgall et al. [2012]
CSF	1.790	Hasgall et al. [2012]	Breast	0.0226	Gabriel et al. [1996a,b,c] (source: breast fat)
Gallbladder	0.900	Gabriel et al. [1996a,b,c]	Bronchi	0.300	Gabriel et al. [1996a,b,c]
Heart-muscle	0.292	Hasgall et al. [2012]	Bronchi lumen	0	Gabriel et al. [1996a,b,c]
Heart-lumen	0.205	Hasgall et al. [2012] (source: blood)	Cerebellum	0.579	Hasgall et al. [2012]
Intervertebral disc	0.171	Gabriel et al. [1996a,b,c]	Commissura anterior	0.369	Hasgall et al. [2012] (source: white matter)
Kidney cortex	0.089	Gabriel et al. [1996a,b,c]	Commissura posterior	0.369	Hasgall et al. [2012] (source: white matter)
Kidney medulla	0.089	Gabriel et al. [1996a,b,c]	Diaphragm	0.286	Hasgall et al. [2012] (source: muscle)
Large intestine	0.055	Gabriel et al. [1996a,b,c]	Ear-cartilage	0.171	Gabriel et al. [1996a,b,c] (source cartilage)
Large intestine lumen	0.286	Gabriel et al. [1996a,b,c] (source: muscle)	Ear-skin	0.100	Dimbylow [2005]
Larynx	0.171	Gabriel et al. [1996a,b,c] (source: cartilage)	Esophagus	0.521	Gabriel et al. [1996a,b,c]
Liver	0.092	Gabriel et al. [2009]	Esophagus lumen	0	Gabriel et al. [1996a,b,c] (source: air)
Lung	0.158	Hasgall et al. [2012] (source: lung inflated)	Eye-vitreous humor	1.500	Gabriel et al. [1996a,b,c]
Marrow red	0.101	Gabriel et al. [1996a,b,c]	Eye-lens	0.200	Gabriel et al. [1996a,b,c]
Meniscus	0.171	Gabriel et al. [1996a,b,c] (source: cartilage)	Hippocampus	0.185	Hasgall et al. [2012] (source: gray matter)
Muscle	0.286	Hasgall et al. [2012]	Hypophysis	0.521	Gabriel et al. [1996a,b,c] (source: glands)
Nerve	0.027	Gabriel et al. [1996a,b,c]	Hypothalamus	0.521	Gabriel et al. [1996a,b,c] (source: glands)
Ovary	0.321	Gabriel et al. [1996a,b,c]	Mandible	0.095	Hasgall et al. [2012] (source: bone)
Pancreas	0.521	Gabriel et al. [1996a,b,c]	Midbrain	0.277	Average gray matter and white matter
Patella	0.095	Hasgall et al. [2012] (source: bone)	Mucosa	0.000427	Gabriel et al. [1996a,b,c]
Skin	0.100	Dimbylow [2005]	Pharynx	0	Gabriel et al. [1996a,b,c]
Small intestine	0.522	Gabriel et al. [1996a,b,c]	Pons	0.277	Average gray matter and white matter
Small intestine lumen	0.286	Hasgall et al. [2012] (source: muscle)	Skull	0.095	Hasgall et al. [2012] (source: bone)
Spinal cord	0.027	Gabriel et al. [1996a,b,c]	Teeth	0.095	Hasgall et al. [2012] (source: bone)
Spleen	0.086	Gabriel et al. [1996a,b,c]	Thalamus	0.185	Hasgall et al. [2012] (source: gray matter)
Stomach	0.521	Gabriel et al. [1996a,b,c]	Tongue	0.271	Gabriel et al. [1996a,b,c]
Stomach lumen	0.233	Gabriel et al. [1996a,b,c]	Trachea	0.301	Gabriel et al. [1996a,b,c]
SAT	0.078	Gabriel et al. [2009] (source: fat)	Trachea-lumen	0	Gabriel et al. [1996a,b,c]
Tendon ligament	0.270	Gabriel et al. [1996a,b,c]	Pineal body	0.521	Gabriel et al. [1996a,b,c] (source: glands)
Thymus	0.521	Gabriel et al. [1996a,b,c]	Medulla-oblongata	0.277	Average gray matter and white matter
Thyroidal gland	0.521	Gabriel et al. [1996a,b,c]	Cornea	0.421	Gabriel et al. [1996a,b,c]
Ureter	0.261	Gabriel et al. [1996a,b,c]	Eye-sclera	0.503	Gabriel et al. [1996a,b,c]
Placenta	0.7	Dimbylow [2006]	Amniotic fluid	1.28; 1.27; 1.10	De Luca et al. [1996], Peyman et al. [2011]

TABLE 2. Fetal Tissue Conductivities

Fetal tissue	σ [S/m]	GA [months]	Fetal tissue	σ [S/m]	GA [months]
Brain	0.185	3; 7; 9	Spinal cord	0.027	3; 7; 9
Bone	0.350	3; 7; 9	Spleen	0.086	3; 7; 9
Eye-lens	0.200	3; 7; 9	Stomach	0.521	3; 7; 9
Eye humor vitreous	1.500	9	Gallbladder	0.900	7; 9
Fat	0.120	3; 7; 9	SAT	0.120	7; 9
Kidney	0.089	3; 7; 9	Adrenal gland	0.521	9
Liver	0.092	3; 7; 9	CSF	1.790	9
Heart muscle	0.292	3; 7; 9	Ovary	0.321	9
Lung	0.158	3; 7; 9	Pancreas	0.521	9
Muscle	0.286	3; 7; 9	Thymus	0.521	9
Bladder	0.205	3; 7; 9	Thyroidal gland	0.521	9
Skin	0.100	3; 7; 9	Esophagus	0.521	9
Intestine	0.522	3; 7; 9	Uterus	0.229	9

at 50 Hz, the basic restriction on the induced current density is intended to protect against acute exposure effects on the central nervous system (CNS) tissues (brain and spinal cord). It is expressed in terms of the peak value (J_{peak}) of the RMS of induced current density, averaged on a surface of 1 cm^2 perpendicular to the direction of current, with a maximum value of 2 mA/m^2. The reference level for the magnetic flux density (B) at 50 Hz refers to the maximum non-perturbed RMS-field level and it is equal to 100 μT. Specifically, in this study, compliance with the basic restrictions has been checked in the fetal CNS tissues (brain and spinal cord).

As to the ICNIRP Guidelines [2010], the physical quantity used to specify the basic restrictions on exposure to EMF is the internal electric field, averaged on a cube of continuous tissue of 2 mm side length. In this case, separate limits are expressed for the CNS tissues of the head and for all the other tissues of the head and body. For a specific tissue, the 99th percentile of the RMS induced electric field is the relevant value to be compared with the basic restriction. At 50 Hz, the basic restriction for the CNS tissues of the head, considering the general public exposure, is 20 mV/m, while for all the other tissues of the head and body, the restriction is 400 mV/m. The reference level for the magnetic flux density (B) at 50 Hz is referring to the maximum non-perturbed RMS-field level and it is equal to 200 μT. In this study, compliance with basic restrictions has been checked for the fetal CNS tissues of the head and for all the other tissues of the head and body, separately.

RESULTS

Grid Resolution Uncertainty Budget

The grid resolution uncertainty budget was evaluated at 7 months GA, changing the fetal tissues grid size from 0.6 to 1.2 mm with a grid step of 0.1 mm. It was assumed that E_{av} and J_{av} are described by a Gaussian normal distribution and the uncertainty was expanded with $k = 2$. Also in this case, a tissue-specific analysis was carried out for $E_{av,99th}$ and $E_{av,peak}$ (Table 3) and for $J_{av,peak}$ (Table 4) for each exposure scenario. The expanded uncertainty in fetal bone tissue is also reported. The uncertainty budget estimated in each tissue shows a maximum of 2.03 dB in fetal SAT tissue for $E_{av,peak}$. Lower peaks are observed in the analysis of $E_{av,99th}$ with values up to 0.46 dB in the fetal gallbladder. As to fetal bone tissue analysis, the uncertainty results were low and less than

TABLE 3. Tissue-Specific Expanded Uncertainty of $E_{av,99th}$ and $E_{av,peak}$ Due to Fetal Grid Resolution for the Three Exposure Scenarios

Exposure scenario	B_{front}	B_{lat}	B_{top}
7mGA fetus, expanded uncertainty (dB)—grid resolution ($E_{av,99th}$ and $E_{av,peak}$)			
Tissue-to-tissue, $E_{av,99th}$	0.32 (gallbladder)	0.30 (skin)	0.46 (gallbladder)
Tissue-to-tissue, $E_{av,peak}$	1 (gallbladder)	2.03 (SAT)	1.26 (muscle)
Bone tissue, $E_{av,99th}$	0.02	0.03	0.05
Bone tissue, $E_{av,peak}$	0.27	0.14	0.06

The maximum of the expanded uncertainty and the tissue, in which it occurs, have been indicated.

TABLE 4. Tissue-Specific Expanded Uncertainty of $J_{av,peak}$ Due to Fetal Grid Resolution for the Three Exposure Scenarios

Exposure scenario	B_{front}	B_{lat}	B_{top}
7mGA fetus, expanded uncertainty (dB)—grid resolution ($J_{av,peak}$)			
Tissue-to-tissue	2.44 (gallbladder)	1.47 (muscle)	2.61 (gallbladder)
Bone tissue	2	0.25	0.09

0.05 dB for $E_{av,99th}$ and 0.27 dB for $E_{av,peak}$. For both metrics, the uncertainty is low; however $E_{av,peak}$ seems to be more sensitive to grid resolution with respect to $E_{av,99th}$. This result is in line with Dawson et al. [2001], in which, through a comparison of various measures of induced electric field in homogenous and layered spheres exposed to uniform magnetic field at 60 Hz obtained with numerical methods, such as SPFD and quasi-static FDTD, and with analytical solutions, it was observed that, for all the numerical methods, the maximum value of the induced electric field was the metric more prone to errors than the other measures. This is due to the singularities introduced by the staircasing smooth surfaces.

The uncertainty budget estimated in the tissue-specific $J_{av,peak}$ shows a maximum of 2.61 dB in the fetal gallbladder. An expanded uncertainty of 2 dB has been found in the bone tissue at B_{front}, which is meaningfully higher than the ones observed in the other two exposure scenarios; however, also in this case, the uncertainty of the grid resolution with respect to $J_{av,peak}$ is low. Therefore, the uncertainty budget analysis confirms the consistency of the results obtained with the grid resolution chosen in this study.

Fetal Exposure to a 1 μT Uniform Magnetic Field at 50 Hz

Figure 3 shows the 50th and 99th percentiles and the peak value of the induced electric field in the whole-body fetus for each incident magnetic field polarization (B_{front}, B_{lat}, and B_{top}) and of the "map" for pregnant women at 3, 7, and 9 months GA, respectively. Figure 3 shows that E_{av} increases with the GA. This is mainly due to the larger fetal dimensions with GA, independently from the fetal posture in the womb and irrespective of the magnetic field direction. This increase is even more evident comparing the "map" E_{av} at each GA: the "map" of the three metrics (50th and 99th percentiles and peak value) is up to three times higher at 9 months GA with respect to the values at 3 months GA, while the difference is up to 50% when comparing 7–9 months GA fetuses.

Observing the trend of $E_{av,99th}$ and $E_{av,peak}$, the incident B_{front} field represents the worst-case exposure scenario at 3 and 9 months GA, whereas the B_{lat} exposure is the worst-case exposure condition for the 7 months GA fetus. At each GA, the difference between $E_{av,99th}$ and $E_{av,peak}$ results is up to 70% (at 7 months GA for B_{top}). This could be due to the fact that the 99th percentile is influenced by the spatial distribution of the induced electric field, by the shape of the tissue, and its discretization and it could underestimate the induced field as already shown in Chen et al. [2013]. The influence of the polarization strongly depends on the fetal shape and position. As an example of differences across the polarizations, at 3 and 7 months GA, $E_{av,50th}$ at B_{front} is about twice the value at B_{lat}.

Figure 4 shows the 50th and 99th percentiles and the peak of the E_{av} estimated in fetal tissues at each GA, considering all the three exposure scenarios previously described (B_{front}, B_{lat}, and B_{top}). At all GAs, fat and skin show high exposure levels for all the polarizations, reaching $E_{av,peak}$ up to 56.86 μV/m in skin tissue for the B_{front} exposure at 9 months GA. The high E field observed in fetal skin tissue is due to the strong contrast in conductivity with the surrounding amniotic fluid (see Table 2). Also $E_{av,99th}$ in the fetal skin tissue is always higher than in the other fetal tissues reaching values up to 38.55 μV/m at 9 months GA.

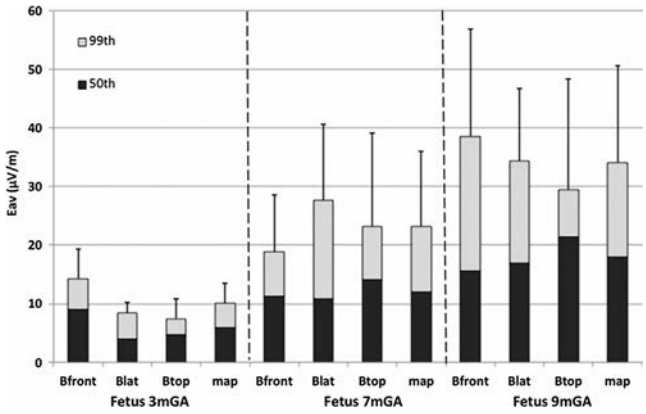

Fig. 3. E_{av} estimated in the whole-body fetus at the three GAs and for the three exposure scenarios (B_{front}, B_{lat}, B_{top}). The mean E_{av} across the polarizations (map) at each GA is also shown. The bars indicate the 50th and 99th percentiles ($E_{av,50th}$, $E_{av,99th}$), whereas the whisker the peak value ($E_{av,peak}$) for B_{front}, B_{lat}, and B_{top}. mGA, month of gestational age; map, mean across the polarizations.

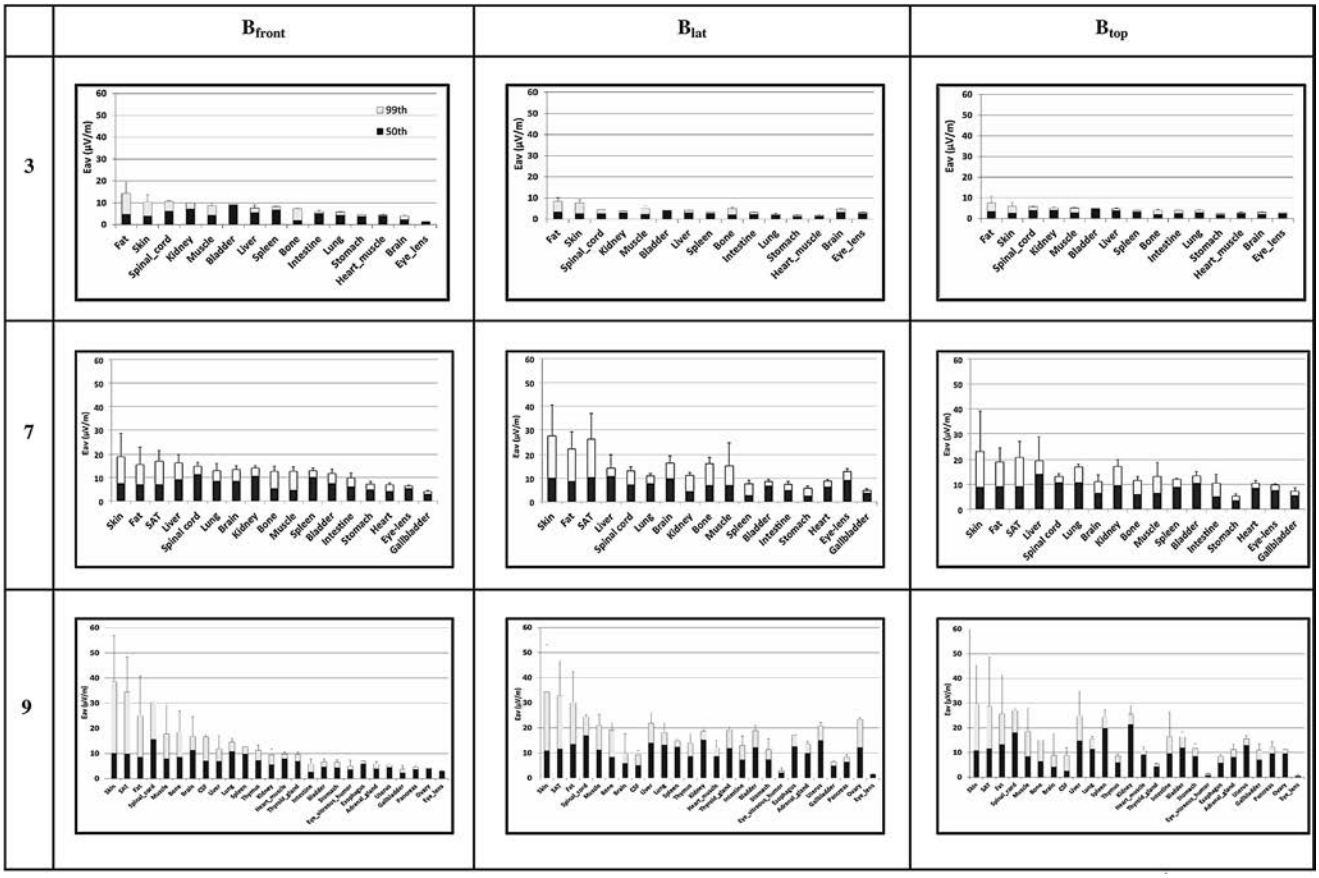

Fig. 4. E_{av} (μV/m) induced in fetal tissues for three exposure scenarios (B_{front}, B_{lat}, B_{top}) at each GA. The bars indicate the 50th and 99th percentiles, whereas the whisker represents the peak value $E_{av,peak}$.

The detailed analysis of each GA shows that, at 3 months, fat and skin are the highest exposed tissue with maximum values of $E_{av,peak}$ equal to 19.33 and 13.66 μV/m, respectively, for the B_{front} exposure. As to the ***B*** field polarization, B_{front} is found to be the worst-case exposure scenario for all fetal tissues at this stage of pregnancy for $E_{av,peak}$. Furthermore B_{front} and B_{top} exposure present similar E_{av} trends in all tissues apart from the stomach.

At 7 and 9 months GA, a worst-case polarization common to all tissues cannot be identified. Moreover, at 7 months GA, skin, fat, subcutaneous adipose tissue (SAT) and liver are the highest exposed tissues for all the polarizations with $E_{av,peak}$ up to 40.57 and 36.89 μV/m for skin and SAT tissues, respectively, while at 9 months GA, skin, SAT, fat, spinal cord, and muscle are the highest exposed tissues for all polarizations.

The effect of polarization increases with the GA (Fig. 4). At 3 and 9 months, large differences are found between the B_{front} and B_{lat} exposures in some specific tissues (e.g., spinal cord, kidney, bladder, intestine), for all the metrics. At 9 months, GA differences, as a function of the polarization, are also observed in adrenal gland, brain, gallbladder, ovary, pancreas and liver with values up to 400% in the same tissue (in ovary tissue) when $E_{av,99th}$ and $E_{av,peak}$ are considered. This means that the exposure of some specific tissues is particularly dependent to the effect of the polarization. The difference between $E_{av,50th}$ and $E_{av,peak}$ increases with GA, with peak values up to four times higher; this is mostly due to the tissue volume over which the induced electric field is averaged and it is meaningful in larger organs. Also the difference between $E_{av,99th}$ and $E_{av,peak}$ increases with GA and it is mostly observed in tissues with large volume (e.g., skin, fat, SAT, muscle, brain, liver), with differences up to 95% of the $E_{av,99th}$ in the brain tissue at 9 months GA.

The results previously discussed about the fetal exposure at each polarization are also confirmed by observing the tissue-specific "map" values for the

TABLE 5. Group of Tissues With Similar Map $E_{av,peak}$ at Each GA

3mGA	7mGA	9mGA
Map $E_{av,peak}$		
Group 1 (≈7 μV/m): spinal cord, muscle	*Group 1* (≈15 μV/m): spinal cord, lung, kidney, bone	*Group 1* (≈27 μV/m): spinal cord, muscle
Group 2 (≈6 μV/m): kidney, bladder, liver, bone	Group 2(≈12 μV/m): spleen, bladder, intestine	*Group 2* (≈18 μV/m): lung, spleen
Group 3 (≈4 μV/m): brain, intestine, lung		*Group 3* (≈12 μV/m): heart-muscle, thyroidal gland, stomach
Group 4 (≈3 μV/m): stomach, heart-muscle		*Group 4* (≈11 μV/m): adrenal gland, esophagus

induced electric field at each GA (Fig. 6, 1st row); these values have been presented to summarize the information about the fetal exposure without taking into account the effect of polarization. In Table 5 the tissues with similar "map" $E_{av,peak}$ are grouped, in order to classify them with respect to level of exposure. These groups of tissues with similar trend of exposure are generally found to be different at each GA, with some exceptions at 3 and 9 months GA.

The same analysis was carried out for the J_{av} distribution in fetal tissues at each GA. In this case, the highest exposed tissues are the ones with high conductivity values, that is, small intestine, gallbladder, and CSF at 3,7, and 9 months GA, respectively. Figure 5 represents the 50th percentile and the peak of the J_{av} induced in fetal tissues at each GA for the three exposure scenarios. In particular, at 3 months GA, intestine and bone present the highest $J_{av,peak}$ values equal to 4.35 and 2.92 μA/m^2, respectively, for the B_{front} exposure, which is the worst-case exposure scenario. In the liver, bladder and spleen the differences between $J_{av,50th}$ and $J_{av,peak}$ in these tissues are up to 20% and lower than in other fetal tissues. At 7 months GA, intestine, bone, gallbladder and muscle have the highest $J_{av,peak}$ up to 8.84 μA/m^2 in gallbladder tissue at B_{top} exposure. Finally, at 9 months GA, CSF, gallbladder and intestine present the highest $J_{av,peak}$ (up to 31.35 μA/m^2 in CSF). For all the exposure scenarios bone tissue presents high $J_{av,peak}$ (up to 7.52 μA/m^2).

Regarding the "map" induced current density (Fig. 6, 2nd row), there are differences in "map" values between tissues at the same GA, as already observed in the E_{av} analysis. These differences increase with GA and are more than three times higher compared to those observed in the E_{av} analysis at 3 and 7 months GA. Also in this case, to summarize the level of exposure at each stage of pregnancy, tissues with similar "map" $J_{av,peak}$ were grouped (Table 6). As previously observed in the analysis of $E_{av,peak}$, the groups of tissues with similar "map" values were different across the stages of pregnancy.

Bone Tissue Analysis

A detailed analysis of bone tissue was performed. As a general comment, when comparing "map" $E_{av,peak}$ in the bone, an increase of 168% from 3 to 7 months GA is found, that decreases to 46% when only the 7 and 9 months GA are compared. This increase with the stage of pregnancy is similar to the one already quantified in the whole-body analysis previously described.

Figure 7 shows the fetal bone E_{av} distributions normalized to the peak value for the worst-case exposure condition (i.e., B_{front} at 3 and 9 months GA and B_{lat} at 7 months GA) at each GA. At 3 months GA, $E_{av,peak}$ has the highest value of 7.76 μV/m on the lumbar vertebrae. $E_{av,peak}$ values are observed on the skull at 7 and 9 months, with maxima of 18.70 and 26.97 μV/m, respectively. At all GAs the maximum electric field is consistently found in other tissues than the bone (see Fig. 4). The differences between "map" $E_{av,99th}$ and "map" $E_{av,peak}$ were found to be as much as 9%, 15%, and 30% at 3, 7, and 9 months GA, respectively. As to J_{av}, $J_{av,peak}$ values were found to be 2.92, 6.57, and 7.52 μA/m^2 at 3, 7, and 9 months GA, respectively. At all GA bone tissue always presents one of the highest values of induced current density among fetal tissues (especially at 3 and 7 months GA, see Fig. 5).

Variation of Fetal Posture at 3 Months GA

Figure 8 presents the three E_{av} distributions in bone tissues for three 3 months GA fetal positions. $E_{av,peak}$ varies in its position in each of the three fetal positions; located in the lumbar vertebrae in the case of posture A with a value of 7.76 μV/m and on the skull in the case of posture B and C, in which $E_{av,peak}$ reaches values up to 8.31 and 10.92 μV/m, respectively. The same distributions are observed for induced current densities, with $J_{av,peak}$ values up to 2.92, 2.89, and 4.13 μA/m^2 for posture A, B, and C, respectively.

The E_{av} dB-variation (Table 7) due to change in fetal posture has been assessed in the tissue-

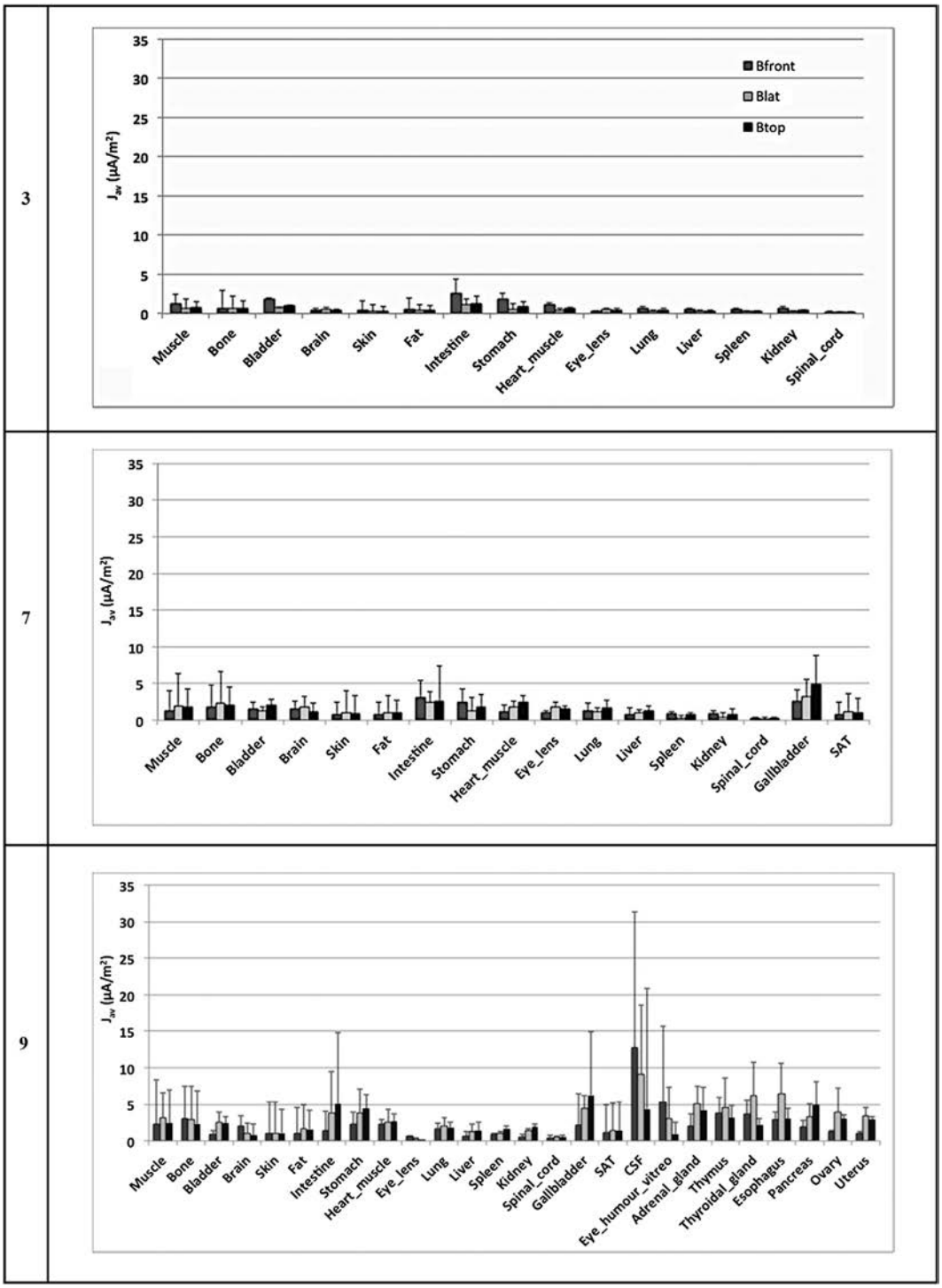

Fig. 5. J_{av} (μA/m^2) induced in fetal tissues for three exposure scenarios (B_{front}, B_{lat}, B_{top}) at each GA. The bar represents the 50th percentile ($J_{av,50th}$), while the whisker is the peak value ($J_{av,peak}$).

specific $E_{av,99th}$ and $E_{av,peak}$ for each exposure scenario (B_{front}, B_{lat}, B_{top}). For both metrics, only the maxima variations are highlighted in the table as well as the specific tissue in which they occur. Furthermore, in a separate row, the variation in fetal bone tissue was reported. In general, the tissue-specific induced electric field presents variation due to the changes in fetal position up to 7 dB in the bladder. This could be due to

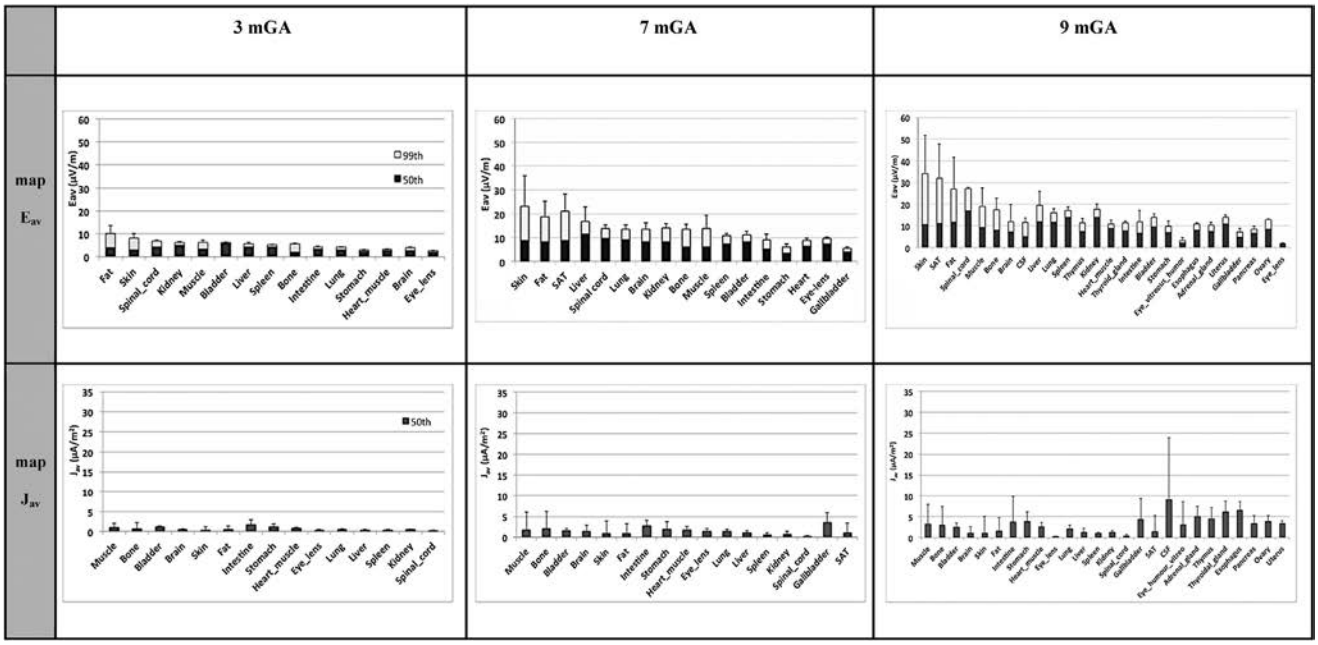

Fig. 6. The mean E_{av} (first row) and mean J_{av} (second row) across the polarizations (map) are represented. In the first row the bars indicate the 50th and 99th percentiles (map $E_{av,50th}$ and map $E_{av,99th}$), while in the second row only the 50th percentile (map $J_{av,50th}$) is represented. For both the whisker represents the peak value (map $E_{av,peak}$ and map $J_{av,peak}$, respectively).

the complexity of the geometrical shape of some organs and tissues, which is influenced more by the incident magnetic field direction and by the position of the fetal tissues with respect to the woman's body. The maximum variation is almost the same for both $E_{av,99th}$ and $E_{av,peak}$. The variation of the induced fields in the bone tissue due to the fetal position results lower with respect the one indicated above, with a maximum of 1.72 dB in $E_{av,99th}$.

Compliance to the ICNIRP Guidelines

In Table 8, the results on compliance of the fetal CNS tissues with the limits recommended by ICNIRP Guidelines [1998] for the general public are reported. J_{peak} in the fetal CNS tissues is always found lower than the limit of 2 mA/m^2 at all GA, with a maximum of 0.49 mA/m^2 at 9 months GA for the B_{front} exposure.

As to compliance with ICNIRP Guidelines [2010] for the general public, Figure 9 shows the maximum $E_{av,99th}$ ($E_{av,99th,max}$) at each GA (including pregnant models with the position of the fetus modified) for each exposure scenario (B_{front}, B_{lat}, and B_{top}). $E_{av,99th,max}$ has been obtained taking the maximum of the tissue-specific $E_{av,99th}$ at each GA, and it has been represented in the figure as percentage of the basic restrictions relative to the fetal CNS tissues of the head (Fig. 9a) and to all the other fetal tissues of the head and body (Fig. 9b), respectively. All fetuses are found in compliance with the basic restrictions for both CNS and PNS tissues (in which all the other tissues of the head and body are included).

TABLE 6. Group of Tissues With Similar Map $J_{av,peak}$ at Each GA

3mGA	7mGA	9mGA
Map $J_{av,peak}$		
Group 1 (≈0.6 μA/m^2): brain, lung	*Group 1* (≈2.7 μA/m^2): brain, heart	*Group 1* (≈6.4 μA/m^2): thymus, thyroidal gland, esophagus
Group 2 (≈1.3 μA/m^2): fat, bladder	*Group 2* (≈2.3 μA/m^2): lung, bladder	*Group 2* (≈2.8 μA/m^2): bladder, brain, lung
Group 3 (≈0.5 μA/m^2): kidney, liver, eye-lens		*Group 3* (≈7.3 μA/m^2): bone, muscle

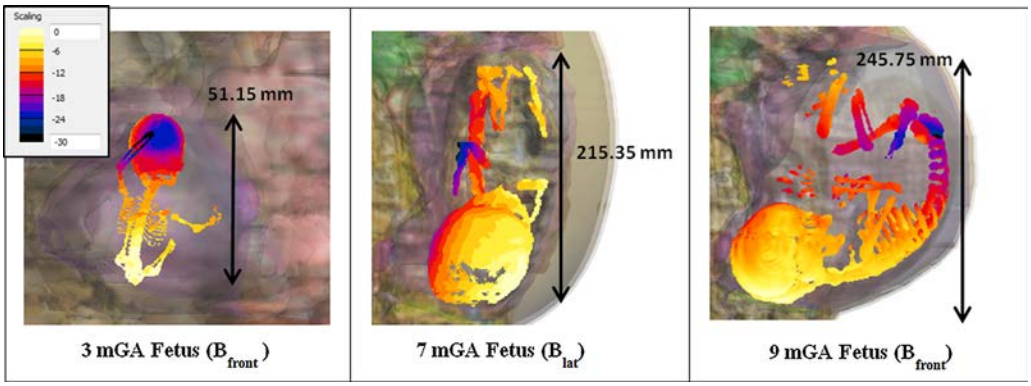

Fig. 7. E_{av} distribution (in dB) in bone tissue at each GA normalized to the peak value of each panel, estimated in the worst-case exposure scenario for each GA (in terms of polarization, as indicated in each panel). Lateral view of the pregnant women is shown.

Indeed, at all GA, $E_{av,99th,max}$ are consistently below the limits suggested by the ICNIRP Guidelines [2010], with a maximum of 23.6% of the basic restriction for the CNS (9 months GA, B_{front}).

DISCUSSION AND CONCLUSIONS

In this study, advanced fetuses in high resolution pregnant woman models at 3, 7, and 9 months GA exposed to uniform magnetic fields with different polarizations of 1 μT of amplitude at 50 Hz has been assessed. In detail, front-to-back, lateral (left-to-right) and top-to-bottom exposure configurations were applied to the woman's body. The fetal whole-body and tissue-specific induced electric field E_{av} averaged on a cube of $2 \times 2 \times 2\,mm^3$ [ICNIRP, 2010], and the induced current density J_{av} averaged on a surface of $1\,cm^2$ perpendicular to the direction of the current [ICNIRP, 1998] were analyzed as a function of GA and magnetic field polarization. An uncertainty evaluation of fetal exposure due to fetal grid discretization was carried out on the 7 months GA fetus. The 50th percentile and peak value were calculated for both J_{av} and E_{av}, and for the latter, the 99th percentile was also analyzed. Fetal exposure was also assessed in terms of the variation of fetal position, by examining two additional pregnant woman models, in which the fetal model assumes two different positions in the woman's womb at 3 months GA (Fig. 2) with respect to the original one. Finally, the results have been scaled to check the compliance to the basic restrictions of the ICNIRP Guidelines [1998, 2010] setting the incident magnetic field to the reference levels of 100 and 200 μT, respectively, at 50 Hz.

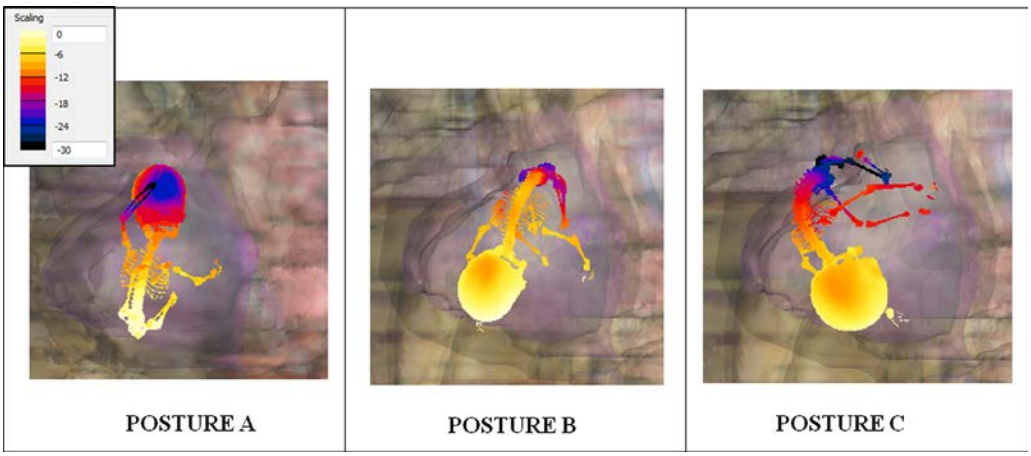

Fig. 8. E_{av} distributions (in dB) in bone tissue at 3 months GA at posture A, B, and C (from Fig. 2) normalized to the peak value of each panel, for the worst-case exposure scenario (B_{front} for all the three postures). Lateral side of the pregnant women is shown.

TABLE 7. $E_{av,99th}$ and $E_{av,peak}$ Variation Due to Change in the Fetal Posture at Each Exposure Scenario

Exposure scenario	B_{front}	B_{lat}	B_{top}
3mGA fetus, variation $E_{av,99th}$ and $E_{av,peak}$ (dB)			
Tissue-to-tissue, $E_{av,99th}$	7 (bladder)	3.80 (stomach)	3.63 (bladder)
Tissue-to-tissue, $E_{av,peak}$	7 (bladder)	3.68 (stomach)	3.61 (bladder)
Bone tissue, $E_{av,99th}$	0.83	0.66	1.72
Bone tissue, $E_{av,peak}$	1.49	0.63	1.70

The consistency of the results, with respect to the grid resolution used in this study, has been assessed by the estimation of the uncertainty budget at 7 months GA, which resulted in low values of expanded uncertainty (i.e., of 0.46 dB in fetal gallbladder for $E_{av,99th}$, of 2.03 dB in fetal SAT for $E_{av,peak}$, and of 2.61 dB in the fetal gallbladder for $J_{av,peak}$).

In general terms, the fetal whole-body E_{av} shows an increment with the stage of pregnancy. This is due to the fact that the fetus is closer to the exterior of the pregnant woman with the growth of fetal size. The maximum level of E_{av} in the fetuses is around 57 μV/m for 1 μT of magnetic flux density B.

Regarding the tissue-specific analysis, in terms of both E_{av} and J_{av}, B_{front} represents the worst-case exposure condition for almost all tissues at 3 months for $E_{av,peak}$, whereas this is not the case for the 7 and 9 months GA where a common worst-case exposure scenario cannot be found for all the tissues. The most exposed tissues in terms of $E_{av,peak}$ are the fat, the skin and the SAT (apart from 3 months GA fetus model, in which the SAT tissue is not segmented), across all polarizations and GAs. Some specific tissues (e.g., spinal cord, kidney, bladder, intestine) are more dependent to the effect of polarization, and this influence increases with GA in the same tissue. Differences up to 95% have been observed between $E_{av,99th}$ and $E_{av,peak}$; thus, $E_{av,99th}$ could underestimate genuine peaks of the induced E_{av} depending more on the induced field distribution as well as on the shape of the tissue. In the J_{av} analysis, the highest exposed tissues are the ones with higher conductivity values, that is, intestine, gallbladder, and CSF at 3, 7, and 9 months GA, respectively. In order to summarize the results, not taking into account the effect of polarization, the "map" values of E_{av} and J_{av} have been calculated for each tissue and at each GA. These values generally confirm the trend of E_{av} and J_{av} already discussed for all GAs.

The induced fields in bone tissue show an increment with the stage of pregnancy similar to the one quantified in whole-body analysis. On average, at all GA, higher $E_{av,peak}$ are found in tissues other than the bone, whereas the latter is one of the fetal tissues with the highest $J_{av,peak}$.

Change in fetal position at 3 months GA dictates fetal exposure variations for both $E_{av,99th}$ and $E_{av,peak}$ (up to 7 dB) in some specific tissues due to change of geometrical shape and the relative position with respect to both incident magnetic field and the woman's body.

Finally, the analysis of the compliance to the ICNIRP Guidelines [1998, 2010] showed that $J_{av,peak}$ in the fetal CNS tissues and $E_{av,99th}$ for all the fetal tissues (CNS and PNS tissues) resulted significantly below the limits. In detail, the maximum $J_{av,peak}$ was 24% with respect to the limit value of 2 mA/m^2 [ICNIRP, 1998] in the fetal CNS tissues, while the $E_{av,99th,max}$ showed values up to 23.6% and 2.7% with respect to the basic restrictions for the CNS and PNS tissues. Furthermore, the $E_{av,peak}$ resulted always in compliance with the basic restrictions of the ICNIRP [2010] at all GAs and polarizations.

Table 9 shows the comparison of the results in the present study with those ones in Dimbylow [2006], Cech et al. [2007], and Zupanic et al. [2007] in terms of $J_{av,peak}$ in whole-body fetus exposed to uniform magnetic fields at 50 Hz for all the three exposure polarizations considered (in the comparison with Zupanic et al. [2007] only B_{front} and B_{lat} exposures have been compared because B_{top} was not available). Specifically in the upper part of Table 9, the comparison was done with Dimbylow [2006], in which the level of magnetic flux density considered was set to 1 mT, forcing the present results to be scaled to the

TABLE 8. RMS J_{peak} in Fetal CNS Tissues, for Each GA and for Each Magnetic Field Polarization (B_{front}, B_{lat}, B_{top})

Fetal CNS tissues	RMS J_{peak} (mA/m^2)		
	3 months GA	7 months GA	9 months GA
B_{front}	0.10	0.37	0.49
B_{lat}	0.11	0.46	0.35
B_{top}	0.07	0.32	0.33

The magnetic field level was set at 100 μT at the frequency of 50 Hz.

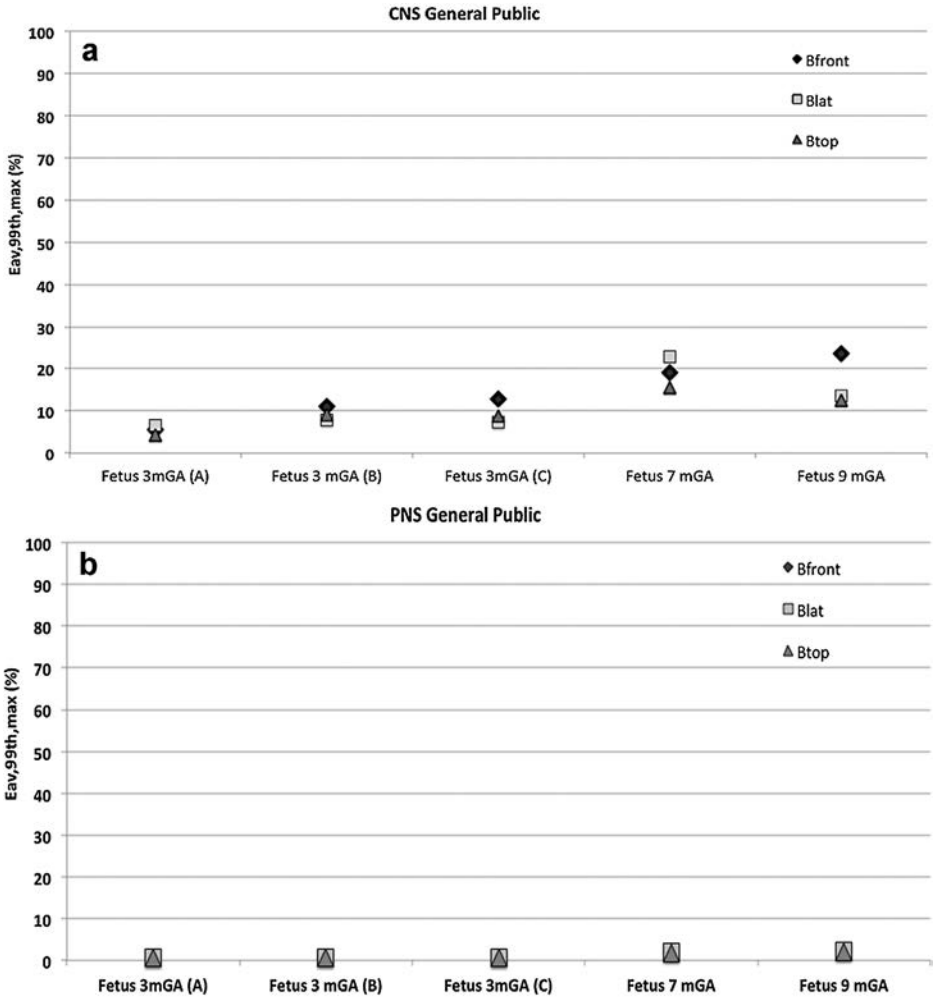

Fig. 9. Maximum fraction of the ICNIRP basic restriction for General Public on the $E_{av,99th}$ ($E_{av,99th,max}$) for the CNS (**a**) and PNS (**b**) exposed to the magnetic fields at the reference level at each GA (including the fetuses with the position changed at 3 months GA) and exposure scenario (B_{front}, B_{lat} and B_{top}). The maximum has been found analyzing each specific fetal tissue at each GA. The reference level of the incident magnetic field was set equal to 200 μT for the general public exposure at 50 Hz.

same level for comparison. One should also note that only results in which the adult conductivities have been assigned to fetal tissues were considered in the table. In general, the increment of $J_{av,peak}$ with GA is observed in both studies; however, $J_{av,peak}$ results are different especially at 7 and 9 months GA. As a possible explanation for the differences, one should take into account the fact that the mass and shape of the fetuses are different, as well as the details of the representation of the fetal organs. Furthermore, some differences in the choice of the dielectric properties for each tissue can also be considered. In particular, the large inequality in the results at 7 and 9 months GA could be accounted for the different details in terms of morphology and tissues between the models used in this study compared to the ones of Dimbylow [2006]. In the lower part of Table 9, the comparison was performed with respect to the results of Cech et al. [2007] and Zupanic et al. [2007]. The results obtained in the present study have been scaled to 100 μT. A direct comparison with these studies cannot be performed because both used a fetus at 30 weeks GA, which is not available in the set of models used in this work. However, the results obtained in this paper at 7 and 9 months of GA (28 and 38 weeks, respectively) could be considered as the lower and upper $J_{av,peak}$ bounds, within which the results in Cech et al. [2007] and Zupanic et al. [2007] fall, even though they seem

TABLE 9. Upper Part: Comparison of $J_{av,peak}$ in Whole-Body Fetus Between Dimbylow [2006] and the Results of This Paper Scaled to an Exposure of 1 mT for All the Three Different Exposure Scenarios (B_{front}, B_{lat}, and B_{top}); Lower Part: Comparison of $J_{av,peak}$ in Whole-Body Fetus Between the Results of This Paper, Scaled to an Exposure of 100 μT, Respectively With Cech et al. [2007] for all the Three Different Exposure Scenarios (B_{front}, B_{lat}, and B_{top}) and Zupanic et al. [2007] for two Exposure Scenarios (B_{front}, B_{lat}); the Gestational Ages and the Masses of the Fetuses Under Comparison are Indicated

	$J_{av,peak}$ in whole-body fetus (mA/m^2)/mT					
	13 weeks—89 g [Dimbylow, 2006]	3 months GA—15 g	26 weeks—1111 g [Dimbylow, 2006]	7 months GA—1700 g	38 weeks—3501 g [Dimbylow, 2006]	9 months GA—2700 g
B_{front}	2.09	4.35	2.93	5.46	4.95	31.35
B_{lat}	1.98	2.20	4.62	6.57	6.83	18.54
B_{top}	1.89	2.28	2.29	8.84	3.71	20.83

	$J_{av,peak}$ in whole-body fetus (mA/m^2) B-field = 100 μT			
	30 weeks [Cech et al., 2007]	30 weeks [Zupanic et al., 2007]	7 months GA—1700 g	9 months GA—2700 g
B_{front}	0.60	0.71	0.55	3.14
B_{lat}	0.65	0.74	0.66	1.85
B_{top}	0.42	—	0.88	2.08

closer to the $J_{av,peak}$ obtained with 7 months GA fetus used in this work.

The aim of this study was not only to improve the knowledge about the human exposure to ELF-MF by means of advanced numerical model with respect to the existing literature, but also giving a dosimetric estimation of the exposure taking into account the MF levels, to which a person is exposed in real life. This is the first paper aiming to analyze in detail, the field distributions in the fetal tissues exposed to the traditional orthogonal polarizations of the *B*-field, following the approach used in the literature.

In conclusion, the use of advanced numerical models of pregnant women at different GA, in which both woman and fetus present a large number of tissues and organs, allowed to accurately quantify the induced fields in the fetal body at 50 Hz, thus building a detailed exposure matrix of fetuses at different stages of pregnancy at 50 Hz. This could be of some help in the evaluation of plausible interaction mechanisms between ELF-MF and health risks by means of biological experiments in vivo, in vitro, and ex vivo.

This study demonstrates that the induced E_{av} in the fetus whole-body increases with GA, but no common worst-case and best-case scenarios across the GA can be identified in terms of the ***B***-field polarization. The highest E_{av} fields were found in the skin and fat, and the highest J_{av} values were found in the CSF due to its high conductivity. The maximum E_{av} and its position in the fetal bone were strongly related to the GA, with large differences found comparing 3 months GA with 7 and 9 months GA. The change in the fetal position in a woman's womb at 3 months GA resulted in interesting variations of E_{av} in some tissues (reaching a maximum of 7 dB in the fetal bladder).

The results obtained in this work not only show compliance with, but also values significantly below the basic restrictions defined in the ICNIRP Guidelines [1998, 2010] at 50 Hz when the incident field is at the action value.

ACKNOWLEDGEMENTS

The software SEMCAD X was provided by SPEAG (Schmid & Partner Engineering AG, Zürich, Switzerland) for research purposes. The authors would also like to thank Helmholtz Zentrum München Deutsches Forschungszentrum für Gesundheit und Umwelt (HMGU, German Research Center for Environmental Health) for the voxel data used in the development of the 9-month-pregnant woman model.

REFERENCES

Ahlbom A, Bridges J, de Seze R, Hillert L, Juutilainen J, Mattsson MO, Neubauer G, Schüz J, Simko M, Bromen K. 2008. Possible effects of electromagnetic fields (EMF) on human health—Opinion of the Scientific Committee on Emerging and Newly Identified Health Risks (SCENIHR). Toxicology 246:248–250.

Ahlbom A, Day N, Feytching M. 2000. A pooled analysis of magnetic fields and childhood leukemia. Br J Cancer 83: 692–698.

Bakker JF, Paulides MM, Neufeld E, Christ A, Chen XL, Kuster N, van Rhoon GC. 2012. Children and adults exposed to low-frequency magnetic fields at the ICNIRP reference levels:

Theoretical assessment of the induced electric fields. Phys Med Biol 57:1815–1829.
Bibin L, Anquez J, Angelini E, Bloch I. 2010. Hybrid 3D pregnant woman and fetus modeling from medical imaging for dosimetry studies. Int J Comput Assist Radiol Surg 5: 49–56.
Brix J, Wettermann H, Scheel O, Feiner F, Matthes R. 2001. Measurements of the individual exposure to 50 Hz and 16 2/3 Hz magnetic fields within the Bavarian population. Bioelectromagnetics 22:323–332.
Cech R, Leitgeb N, Pediaditis M. 2007. Fetal exposure to low frequency electric and magnetic fields. Phys Med Biol 52:879–888.
Chen X-L, Benkler S, Chavannes N, De Santis V, Bakker J, van Rhoon G, Mosig J, Kuster N. 2013. Analysis of human brain exposure to low-frequency magnetic fields: A numerical assessment of spatially averaged electric fields and exposure limits. Bioelectromagnetics 34:375–384.
Chiu RS, Stuchly MA. 2005. Electric fields in bone marrow substructures at power-line frequencies. IEEE Trans Biomed Eng 52:1103–1109.
Christ A, Guldimann R, Büehlmann B, Zefferer M, Bakker JF, van Rhoon GC, Kuster N. 2012. Exposure of the human body to professional and domestic induction cooktops compared to the basic restrictions. Bioelectromagnetics 33:695–705.
Christ A, Kainz W, Hahn EG, Honegger K, Zefferer M, Neufeld E, Rascher W, Janka R, Bautz W, Chen J, Kiefer B, Scmitt P, Hollenbach HP, Shen J, Oberle M, Szezerba D, Kam A, Guag JW, Kuster N. 2010. The virtual family-development of surface-based anatomical models of two adults and two children for dosimetric simulations. Phys Med Biol 55: 23–38.
Dawson TW, Potter M, Stuchly MA. 2001. Evaluation of modeling accuracy of power frequency field interactions with the human body. Appl Comput Electromag Soc J 16: 162–172.
De Luca F, Cametti C, Zimatore G, Maraviglia B, Pachi A. 1996. Use of low-frequency electrical impedance measurements to determine phospholipid content in amniotic fluid. Phys Med Biol 41:1863–1869.
Dimbylow P. 2002. Fine resolution calculation of SAR in the human body for frequencies up to 3 GHz. Phys Med Biol 47:2835–2846.
Dimbylow P. 2005. Development of the female voxel phantom, NAOMI, and its application to calculations of induced current densities and electric fields from applied low frequency magnetic and electric fields. Phys Med Biol 50:1047–1070.
Dimbylow P. 2006. Development of pregnant female, hybrid voxel-mathematical models and their application to the dosimetry of applied magnetic and electric fields at 50 Hz. Phys Med Biol 51:2383–2394.
Dimbylow P, Findlay R. 2010. The effects of body posture, anatomy, age and pregnancy on the calculation of induced current densities at 50 Hz. Radiat Prot Dosim 139:532–535.
Gabriel C, Gabriel S, Corthout E. 1996a. The dielectric properties of biological tissues: 1. Literature survey. Phys Med Biol 41:2231–2249.
Gabriel S, Lau RW, Gabriel C. 1996b. The dielectric properties of biological tissues: 2. Measurements in the frequency range 10 Hz to 20 GHz. Phys Med Biol 41:2251–2269.
Gabriel S, Lau RW, Gabriel C. 1996c. The dielectric properties of biological tissues: 3. Parametric models for the dielectric spectrum of tissues. Phys Med Biol 41:2271–2293.
Gabriel C, Peyman A, Grant EH. 2009. Electrical conductivity of tissue at frequencies below 1 MHz. Phys Med Biol 54:4863–4878.
Gandhi OP, Kang G, Wu D, Lazzi G. 2001. Currents induced in anatomic models of the human for uniform and non-uniform power frequency magnetic fields. Bioelectromagnetics 22: 112–121.
Greenland S, Sheppard AR, Kaune WT, Poole C, Kelsh MA. 2000. A pooled analysis of magnetic fields, wire codes, and childhood leukemia. Epidemiology 11:624–634.
Grellier J, Ravazzani P, Cardis E. 2014. Potential health impacts of residential exposures to extremely low frequency magnetic fields in Europe. Environ Int 62:55–63.
Hand JW, Li Y, Thomas EL, Rutherford MA, Hajnal JV. 2006. Prediction of specific absorption rate in mother and fetus associated with MRI examinations during pregnancy. Magn Reson Med 55:883–893.
Hasgall PA, Neufeld E, Gosselin MC, Klingenböck A, Kuster N. 2012. IT'IS Database for thermal and electromagnetic parameters of biological tissues Version 2.2, July 11th, Available from: www.itis.ethz.ch/database. (Last accessed February 2014).
Hirata A, Caputa K, Dawson TW, Stuchly MA. 2001. Dosimetry in models of child and adult for low-frequency electric field. IEEE Trans Biomed Eng 48:1007–1012.
ICNIRP. 2010. Guidelines for limiting exposure to time-varying electric and magnetic fields (1 Hz to 100 kHz). Health Phys 99:818–836.
International Commission on Non-ionizing Radiation Protection (ICNIRP). 1998. Guidelines for limiting exposure to time-varying electric, magnetic and electromagnetic fields (up to 300 GHz). Health Phys 74:494–522.
International Organization for Standardization (ISO)/International Electrotechnical Commission (IEC) Guide. 98-3: 2008. Uncertainty of measurement part 3: Guide to the expression of uncertainty in measurement (gum:1995). Geneva, Switzerland: ISO.
Kainz W, Chan DD, Casamento JP, Bassen HI. 2003. Calculation of induced current densities and specific absorption rates (SAR) for pregnant women exposed to hand-held metal detectors. Phys Med Biol 28:2551–2560.
Kheifets L, Ahlbom A, Crespi CM, Draper G, Hagihara J, Lowenthal RM, Mezei G, Oksuzyan S, Schüz J, Swanson J, Tittarelli A, Vinceti M, Wunsch Filho V. 2010. Pooled analysis on recent studies on magnetic fields and childhood leukemia. Br J Cancer 103:1128–1135.
Leitgeb N, Cech R, Schroettner J. 2008. Assessment of inhomogeneus magnetic fields exposure. Radiat Prot Dosim 131:251–258.
Liorni I, Parazzini M, Fiocchi S, Ravazzani P. 2013. Exposure of high resolution fetuses in advanced pregnant woman models to uniform magnetic fields at the frequency of 50 Hz. Conference Proceedings IEEE Engineering in Medicine and Biology Society 2013: 4525–4528.
Nagaoka T, Togashi T, Saito K, Takahashi M, Ito K, Watanabe S. 2007. An anatomically realistic whole-body pregnant-woman model and specific absorption rates for pregnant-woman exposure to electromagnetic plane waves from 10 MHz to 2 GHz. Phys Med Biol 52:6731–6745.
Peyman A, Gabriel C, Benedickter HR, Fröhlich J. 2011. Dielectric properties of human placenta, umbilical cord and amniotic fluid. Phys Med Biol 56:N93–N98.
Peyman A, Gabriel C, Grant EH, Vermeeren G, Martens L. 2009. Variation of the dielectric properties of tissues with age: The effect on the values of SAR in children when exposed to walkie-talkie devices. Phys Med Biol 54:227–241.

Pui CH, Robinson LL, Look AT. 2008. Acute lymphoblastic leukemia. Lancet 371:1030–1043.

Schüz J, Ahlbom A. 2008. Exposure to electromagnetic fields and the risk of childhood leukaemia: A review. Radiat Prot Dosim 132:202–211.

Schüz J, Grigat JP, Störmer B, Rippin G, Brinkmann K, Michaelis J. 2000. Extremely low frequency magnetic fields in residences in Germany. Distribution of measurements, comparison of two methods for assessing exposure, and predictors for the occurrence of magnetic fields above background level. Radiat Environ Biophys 39: 233–240.

Shi C, Xu XG. 2004. Development of a 30-week-pregnant female tomographic model from computed tomography (CT) images for Monte Carlo organ dose calculations. Med Phys 31:2491–2497.

Taylor BN, Kuyatt CE. 1994. Guidelines for evaluating and expressing the uncertainty of NIST measurement results. NIST Technical Note 1297. Washington: Government Printing Office.

World Health Organization (WHO). 2007a. Extremely low frequency fields. Environmental Health Criteria. Vol. 238. Geneva, Switzerland: World Health Organization Press.

World Health Organization (WHO). 2007b. Research agenda for extremely low frequency fields. Geneva, Switzerland. http://www.who.int/peh-emf/research/elf_research_agenda_2007.pdf. [Last Accessed December 2013].

Xu XG, Taranenko V, Zhang J, Shi C. 2007. A boundary-representation method for designing whole-body radiation dosimetry models: Pregnant females at the ends of three gestational periods—RPI-P3, -P6 and -P9. Phys Med Biol 52:7023–7044.

Zoppetti N, Andreuccetti D, Bellieni C, Bogi A, Pinto I. 2011. Evaluation and characterization of fetal exposures to low frequency magnetic fields generated by laptop computers. Prog Biophys Mol Biol 107:456–463.

Zupanic A, Valic B, Miklavcic D. 2007. Numerical assessment of induced current densities for pregnant women exposed to 50 Hz electromagnetic field. Int Fed Med Biol Eng Proc 16:226–229.